Nonclassical effects in photon statistics of atomic optical bistability

Daniel Erenso, Ron Adams, Hua Deng, Reeta Vyas, and Surendra Singh
Department of Physics, University of Arkansas, Fayetteville, Arkansas 72701

(Received 30 May 2001; published 13 September 2001)

Homodyne statistics of light generated by an atomic system exhibiting optical bistability are analyzed. Using the dynamical equations of motion for a single atom in a coherently driven cavity in the good cavity limit, we show that the homodyne field can be described in terms of two independent real Gaussian stochastic processes and a coherent component. By making a Karhunen-Loève expansion of the field variables we derive the generating function for the photoelectron statistics. From this generating function photoelectron-counting distribution, factorial moments, and waiting-time distribution are obtained analytically. These quantities are directly measurable in photon-counting experiments. We show that the homodyne field exhibits many interesting nonclassical features including nonclassical effects in higher-order factorial moments.

DOI: 10.1103/PhysRevA.64.043806 PACS number(s): 42.50.Ar, 42.50.Dv, 42.50.Ct

I. INTRODUCTION

Interaction of a single two-level atom with a quantum field inside a coherently driven cavity in the good cavity limit, is known to show optical bistability [1,2]. We will refer to this system as single atom optical bistability (SAOB). Similarly, N two-level atoms placed inside a coherently driven cavity also exhibit optical bistability that we shall refer to as multiatom optical bistability (MAOB) [3,4]. These systems are also known to show antibunching, although the size of antibunching is small. In order to enhance antibunching and other nonclassical effects, several schemes based on interference [5], passive filter cavities [6], or homodyne detection [7] have been proposed.

Homodyning a field with a coherent local oscillator (LO) provides one way of enhancing nonclassical effects. The homodyne field can exhibit strong nonclassical features, which are not shown by the original field. The homodyne statistics are sensitive to the phase difference between the signal and the LO. An example of this behavior is provided by the light from the degenerate parametric oscillator, which is highly bunched and super-Poissonian. When this field is homodyned with a LO, the homodyne field shows a variety of nonclassical effects such as antibunching, sub-Poissonian statistics, and violation of other classical inequalities [8–10].

In this paper we consider homodyning of the light from a system that exhibits SAOB with the light beam from a LO at a lossless beam splitter as shown in Fig. 1. A detector of efficiency η placed at one of the output ports of the beam splitter detects the homodyne field and generates photoelectric pulses, which are measured by suitable electronics. We study photoelectron statistics measured by the detector. In Sec. II we start from the equations of motion derived by Wang and Vyas for a single two-level atom in the good cavity limit [2] and show that the field from the SAOB can be expressed in terms of two Gaussian random variables. We then derive the equations that govern the dynamics of the homodyne field. Using these equations and applying the Karhunen-Loève expansion for the field variables, we calculate the moment generating function for the photocount distribution. We also show that a system exhibiting MAOB can also be described by similar expressions with an appropriate change in parameters. In Sec. III we present an analytic expression for the moment generating function. Photon statistics of the homodyne field are then analyzed with the help of the moment generating function. The photocount distribution, its moments, and the waiting-time distribution for the homodyne field are calculated. Finally, in Sec. VI, a summary of the main results of the paper is presented.

II. DYNAMICS OF THE HOMODYNE FIELD AND THE GENERATING FUNCTION

In this section we derive equations of motion describing the dynamics of the homodyne field when the signal is from the SAOB. We will see that similar equations are obtained when the signal is from the MAOB.

Consider a single damped two-level atom with transition frequency ω_a, interacting with a single mode of a cavity with resonance frequency ω_c. The cavity is driven by a coherent external field of frequency ω_o and amplitude ϵ. In the electric dipole and rotating-wave approximation, the Hamiltonian for this system can be written as

$$\hat{H}=\omega_a\hat{\sigma}_z+\hbar\omega_c\hat{a}^\dagger\hat{a}+ig\hbar(\hat{a}^\dagger\hat{\sigma}_-+\hat{a}\hat{\sigma}_+)+i\hbar\epsilon(\hat{a}^\dagger e^{-i\omega_o t}-\hat{a}e^{i\omega_o t})+\hat{H}_{loss}. \tag{1}$$

Here $\hat{a}$ and $\hat{a}^\dagger$ are the annihilation and creation operators for the cavity mode, $\hat{\sigma}_+$, $\hat{\sigma}_-$, and $\hat{\sigma}_z$ are the Pauli spin matrices describing the two-level atom, g is the atom-field coupling constant, and $\hat{H}_{loss}$ describes atomic losses due to spontaneous decay and field losses at the cavity mirrors.

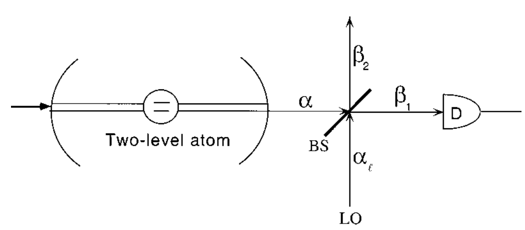

FIG. 1. System for homodyning the SAOB field with the LO field. BS denotes the beam splitter and D denotes a detector.

Using the Hamiltonian of Eq. (1), Wang and Vyas derived a Fokker-Planck equation without using system size expansion [11]. This gives a set of Îto stochastic differential equations for the atomic and field variables. In the good cavity limit, in which atomic variables decay much faster than the cavity field variables, it is possible to eliminate atomic variables adiabatically. In this approximation the following equations govern the time evolution of the cavity field [2]:

$$\dot{\alpha}=-\gamma(1+i\delta_c)\alpha-\frac{2\gamma C(1-i\delta_a)}{1+\delta_a^2+\alpha\alpha_*/n_0}\alpha+\epsilon+\Gamma(t), \quad (2)$$

$$\dot{\alpha}_*=-\gamma(1-i\delta_c)\alpha_*-\frac{2\gamma C(1+i\delta_a)}{1+\delta_a^2+\alpha\alpha_*/n_0}\alpha_*+\epsilon+\Gamma_*(t), \quad (3)$$

where α and α_* are complex field amplitudes corresponding to $\hat{a}$ and $\hat{a}^\dagger$ in the positive-P representation [12], $\delta_a=2(\omega_a-\omega_o)/\gamma_a$ and $\delta_c=(\omega_c-\omega_o)/\gamma$ are the atomic and cavity detuning parameters, 2γ is the cavity field decay rate, γ_a is the spontaneous emission rate to modes other than the privileged cavity mode, $C\,[=g^2/(\gamma_a\gamma)]$ is the cooperativity parameter, and $n_0\ [=\gamma_a^2/(8g^2)]$ is the saturation photon number. In the positive-P representation, α and α_* may not be the complex conjugate of each other. $\Gamma(t)$ and $\Gamma_*(t)$ are delta correlated Gaussian noise processes with

$$\begin{aligned}\langle\Gamma(t)\Gamma(t')\rangle&=\langle\Gamma_*(t)\Gamma_*(t')\rangle^*\\&=-\frac{2\gamma C(\alpha^2/n_0)}{(1+\delta_a^2+\alpha\alpha_*/n_0)^3}\left[(1-i\delta_a)^3\right.\\&\quad\left.+\frac{1}{2}(\alpha\alpha_*/n_0)^2\right]\delta(t-t'), \end{aligned}\quad (4)$$

$$\begin{aligned}\langle\Gamma(t)\Gamma_*(t')\rangle&=\langle\Gamma_*(t)\Gamma(t')\rangle\\&=\frac{2\gamma C(\alpha\alpha_*/n_0)^2}{(1+\delta_a^2+\alpha\alpha_*/n_0)^3}\\&\quad\times\left[2+\frac{1}{2}(\alpha\alpha_*/n_0)\right]\delta(t-t'). \end{aligned}\quad (5)$$

It is interesting to note that the dynamics of the cavity field for the MAOB [3,4] for the case of equal radiative and collisional damping are also described by Eqs. (2) and (3), which have been derived for the SAOB [2]. For the MAOB, however, the atomic cooperativity parameter is modified to be $C=Ng^2/\gamma_a\gamma$, where N is number of atoms in the cavity. With this redefinition of the cooperativity parameter, the results of this paper also apply to the MAOB.

For zero atomic and cavity detunings we expand α and α_* about the steady-state amplitudes $\sqrt{n_0\bar{n}}$ as

$$\alpha=\sqrt{n_0}[\sqrt{\bar{n}}+\delta\alpha], \quad \alpha_*=\sqrt{n_0}[\sqrt{\bar{n}}+\delta\alpha_*], \quad (6)$$

where $\delta\alpha$ and $\delta\alpha_*$ are small deviations from the steady-state amplitudes, $\bar{n}$ is the mean photon number in units of the saturation photon number n_0, and it is determined by $(\epsilon/\gamma)^2=n_0\bar{n}[1+2C/(1+\bar{n})]^2$. An analysis of the steady-state solutions of Eqs. (2) and (3), as a function of the driving field amplitude, indicates that for zero atomic and cavity detunings, optical bistability may exist for $C>4$. In this region, for a given driving field amplitude and cooperativity parameter, the system can jump to any one of the two possible stable branches. The unstable branch or the curve for the mean photon number $\bar{n}$ in the range $[C-1-\sqrt{C(C-4)}]\geqslant\bar{n}\geqslant[C-1+\sqrt{C(C-4)}]$, is forbidden. The range of $\bar{n}$ corresponding to the two stable branches is $0<\bar{n}<[C-1-\sqrt{C(C-4)}]$, or $\bar{n}>[C-1+\sqrt{C(C-4)}]$.

Substituting Eq. (6) in Eqs. (2) and (3) and linearizing these equations, we obtain a set of coupled stochastic differential equations

$$\dot{\delta\alpha}=-a_1\delta\alpha-a_2\delta\alpha_*+c_1\xi_1(t)+c_2\xi_2(t), \quad (7)$$

$$\dot{\delta\alpha}_*=-a_2\delta\alpha-a_1\delta\alpha_*+c_2\xi_1(t)+c_1\xi_2(t), \quad (8)$$

where

$$a_1=\gamma\left(1+\frac{2C}{(1+\bar{n})^2}\right), \quad a_2=\frac{-2\gamma C\bar{n}}{(1+\bar{n})^2}, \quad (9)$$

$$c_1=\frac{i}{2\sqrt{n_0}}\left[\sqrt{\frac{2\gamma C\bar{n}(1-2\bar{n})}{(1+\bar{n})^3}}+\sqrt{\frac{2\gamma C\bar{n}}{1+\bar{n}}}\right], \quad (10)$$

$$c_2=\frac{i}{2\sqrt{n_0}}\left[\sqrt{\frac{2\gamma C\bar{n}(1-2\bar{n})}{(1+\bar{n})^3}}-\sqrt{\frac{2\gamma C\bar{n}}{1+\bar{n}}}\right]. \quad (11)$$

Here $\xi_1(t)$ and $\xi_2(t)$ are statistically independent Gaussian white-noise processes with zero mean and correlations

$$\langle\xi_i(t)\xi_j(t')\rangle=\delta_{ij}\delta(t-t'). \quad (12)$$

Note that c_1 and c_2 are pure imaginary for $\bar{n}<1/2$, and complex for $\bar{n}>1/2$. For $\bar{n}<1/2$ we can introduce the variables

$$\delta\alpha=i(u_1+u_2), \quad \delta\alpha_*=i(u_1-u_2), \quad (13)$$

to decouple Eqs. (7) and (8). Using these variables in Eqs. (7) and (8), we obtain two uncoupled equations for u_1 and u_2,

$$\dot{u}_i=-\lambda_i u_i+b_i q_i, \quad i=1,2, \quad (14)$$

where

$$\lambda_1=\gamma\left(1+\frac{2C(1-\bar{n})}{(1+\bar{n})^2}\right), \quad \lambda_2=\gamma\left(1+\frac{2C}{1+\bar{n}}\right), \quad (15)$$

$$b_1=\sqrt{\frac{\gamma C\bar{n}(1-2\bar{n})}{n_0(1+\bar{n})^3}}, \quad b_2=\sqrt{\frac{\gamma C\bar{n}}{n_0(1+\bar{n})}}. \quad (16)$$

Here q_1 and q_2 are independent delta correlated Gaussian white-noise processes with unit strength. By solving the differential equation (14), we can show that u_1 and u_2 are independent real Gaussian random processes with zero mean and correlations given by

$$\langle u_1(t)u_1(t')\rangle = \frac{\gamma C\bar{n}(1-2\bar{n})}{2n_0(1+\bar{n})^3\lambda_1} e^{-\lambda_1|t-t'|}, \tag{17}$$

$$\langle u_2(t)u_2(t')\rangle = \frac{\gamma C\bar{n}}{2n_0(1+\bar{n})\lambda_2} e^{-\lambda_2|t-t'|}. \tag{18}$$

Gaussian variables u_1 and u_2 govern the dynamics of the field emitted by the cavity.

We now use u_1 and u_2 to express the homodyne field, which is obtained by superposing the light from the SAOB and the LO at a lossless beam splitter. The beam splitter is characterized by power transmitivity $\mathcal{T}$ and reflectivity $\mathcal{R}$ with the condition $\mathcal{T}+\mathcal{R}=1$. In the positive-$P$ representation [12], the complex field amplitudes β_i and β_{i*}, corresponding to the annihilation and creation operators at the output ports of the beam splitter, can be written as

$$\beta_1 = \alpha\sqrt{\mathcal{T}} + |\alpha_l| e^{i\phi}\sqrt{\mathcal{R}}, \quad \beta_{1*} = \alpha_*\sqrt{\mathcal{T}} + |\alpha_l| e^{-i\phi}\sqrt{\mathcal{R}}, \tag{19}$$

$$\beta_2 = |\alpha_l| e^{i\phi}\sqrt{\mathcal{T}} - \alpha\sqrt{\mathcal{R}}, \quad \beta_{2*} = |\alpha_l| e^{-i\phi}\sqrt{\mathcal{T}} - \alpha_*\sqrt{\mathcal{R}}, \tag{20}$$

where α and α_* are the complex field amplitudes corresponding to the annihilation and creation operators for the SAOB field, $|\alpha_l|$ is the LO field amplitude, and ϕ is the LO phase relative to the SAOB. Here we will focus our attention on the β_1 port of the beam splitter. Results for the β_2 port can be obtained by replacing $\sqrt{\mathcal{R}}$ by $\sqrt{\mathcal{T}}$ and $\sqrt{\mathcal{T}}$ by $-\sqrt{\mathcal{R}}$. Using Eqs. (6) and (13) we can express β_1 and β_2 as

$$\beta_1 = \sqrt{n_0}[\sqrt{\bar{n}} + i(u_1+u_2)\sqrt{\mathcal{T}} + \sqrt{\bar{n}_l} e^{i\phi}\sqrt{\mathcal{R}}], \tag{21}$$

$$\beta_{1*} = \sqrt{n_0}[\sqrt{\bar{n}} + i(u_1-u_2)\sqrt{\mathcal{T}} + \sqrt{\bar{n}_l} e^{-i\phi}\sqrt{\mathcal{R}}], \tag{22}$$

where $|\alpha_l| = \sqrt{n_0\bar{n}_l}$. Equations (21) and (22) describe the homodyne field. We use these equations to derive the generating function, which will be used to study the photon statistics of the homodyne field.

In the positive-P representation the time ordered and normally ordered generating function $G(s,T)$ for the photon-counting distribution can be written as

$$G(s,T) = \left\langle \exp\left[-s\eta \int_0^T I(t)dt \right] \right\rangle, \tag{23}$$

where $0 \leqslant \eta \leqslant 1$ is the quantum efficiency of detection, T is the counting time, and s is an auxiliary parameter. The photon number flux variable $I(t)$ for the homodyne field for $\bar{n} < 1/2$, is given by

$$\begin{aligned} I(t) &= 2\gamma(\beta_1\beta_{1*}) \\ &= 2\gamma n_0\{(u_2\sqrt{\mathcal{T}} + \sqrt{\bar{n}_l}\sqrt{\mathcal{R}}\sin\phi)^2 \\ &\quad - [u_1\sqrt{\mathcal{T}} - i(\sqrt{\bar{n}}\sqrt{\mathcal{T}} + \sqrt{\bar{n}_l}\sqrt{\mathcal{R}}\cos\phi)]^2\}, \end{aligned} \tag{24}$$

where we have used Eqs. (21) and (22). Thus averaging in Eq. (23) is with respect to the variables u_1 and u_2.

As mentioned earlier, c_1 and c_2 in Eqs. (10) and (11) are complex for $\bar{n} > 1/2$. For $\bar{n} > 1/2$, we introduce the variables

$$\delta\alpha = (v_1 + iv_2), \quad \delta\alpha_* = (v_1 - iv_2) \tag{25}$$

in Eqs. (7) and (8) and find that v_1 and v_2 are independent real Gaussian random processes with zero mean and correlations

$$\langle v_1(t)v_1(t')\rangle = \frac{\gamma C\bar{n}(2\bar{n}-1)}{2n_0(1+\bar{n})^3\lambda_1} e^{-\lambda_1|t-t'|}, \tag{26}$$

$$\langle v_2(t)v_2(t')\rangle = \frac{\gamma C\bar{n}}{2n_0(1+\bar{n})\lambda_2} e^{-\lambda_2|t-t'|}. \tag{27}$$

Thus for $\bar{n} > 1/2$, the photon number flux variable $I(t)$ for the homodyne field is given by

$$\begin{aligned} I(t) = 2\gamma n_0\{&[v_1\sqrt{\mathcal{T}} + (\sqrt{\bar{n}}\sqrt{\mathcal{T}} + \sqrt{\bar{n}_l}\sqrt{\mathcal{R}}\cos\phi)]^2 + (v_2\sqrt{\mathcal{T}} \\ &+ \sqrt{\bar{n}_l}\sqrt{\mathcal{R}}\sin\phi)^2\}. \end{aligned} \tag{28}$$

Thus $I(t)$ for the HSAOB for $\bar{n} > 1/2$ can be expressed as the sum of the squares of two Gaussian random processes with different variances. Note that $I(t)$ for thermal light is also expressible as a sum of the squares of the two Gaussian random processes, which have the same variance. On the other hand, $I(t)$ for $\bar{n} < 1/2$ in Eq. (24) is expressed as a difference of the squares of Gaussian random processes. This difference gives rise to interesting nonclassical effects for $\bar{n} < 1/2$, which we do not see for $\bar{n} > 1/2$ or thermal light.

Substituting the expression for $I(t)$ in Eq. (23), and making a Karhunen-Loève expansion of u_1 and u_2 for $\bar{n} < 1/2$ and v_1 and v_2 for $\bar{n} > 1/2$, and following the method outlined in Ref. [8], we obtain the generating function in a closed form:

$$G(s,T) = Q_1(s,T)e^{-f_1(s,T)}Q_2(s,T)e^{-f_2(s,T)}, \tag{29}$$

where

$$Q_i(s,T) = \frac{e^{\lambda_i T/2}}{[\cosh(z_i T) + 1/2(\lambda_i/z_i + z_i/\lambda_i)\sinh(z_i T)]^{1/2}}, \tag{30}$$

$$f_i(s,T)=K_iT\left[\frac{\lambda_i^2}{z_i^2}\left(1+\frac{2}{2+\lambda_iT}\right)+\frac{2}{\lambda_iB_iT^2+(2B_i-\lambda_i)T-2}-\left(\frac{2B_i\lambda_i}{z_i^2}\right)\frac{\mathcal{C}(z_i)}{B_iT-1}\right], \tag{31}$$

$$\mathcal{C}(z_i)=\frac{\cosh(z_iT/2)+(\lambda_i/z_i)(1+2/\lambda_iT)\sinh(z_iT/2)}{\cosh(z_iT/2)+(z_i/\lambda_i)\sinh(z_iT/2)} \tag{32}$$

for $i=1,2$ and

$$z_1^2=\lambda_1^2-2s\,\eta\mathcal{T}\gamma^2 2C\frac{\overline{n}(1-2\overline{n})}{(1+\overline{n})^3}, \tag{33}$$

$$z_2^2=\lambda_2^2+2s\,\eta\mathcal{T}\gamma^2 2C\frac{\overline{n}}{(1+\overline{n})}, \tag{34}$$

$$B_1=-s\,\eta\mathcal{T}\gamma^2 2C\frac{\overline{n}(1-2\overline{n})}{\lambda_1(1+\overline{n})^3}, \tag{35}$$

$$B_2=s\,\eta\mathcal{T}\gamma^2 2C\frac{\overline{n}}{\lambda_2(1+\overline{n})}, \tag{36}$$

$$K_1=2\gamma s\,\eta n_0[\sqrt{\overline{n}}\sqrt{\mathcal{T}}+\sqrt{\overline{n}_l}\sqrt{\mathcal{R}}\cos\phi]^2, \tag{37}$$

$$K_2=2\gamma s\,\eta n_0\overline{n}_l\mathcal{R}\sin^2\phi. \tag{38}$$

We use this generating function to study photoelectron statistics of the homodyned field.

III. PHOTOELECTRON-COUNTING STATISTICS

Homodyne light incident on the detector D generates photoelectric pulses. Statistics of these pulses can be described in terms of the photoelectron-counting distribution, its factorial moments, and the waiting-time distribution. In the following section we derive these quantities using the generating function obtained in the previous section.

A. Photoelectron-counting distribution and factorial moments

The photoelectron-counting distribution $p(m,T)$ is the probability of counting m photoelectric pulses in the time interval T. It is obtained by differentiating the generating function $G(s,T)$ m times with respect to s,

$$p(m,T)=\frac{(-1)^m}{m!}\left[\frac{d^m}{ds^m}G(s,T)\right]_{s=1}. \tag{39}$$

Substituting the expression for $G(s,T)$ from Eq. (29) into Eq. (39), and applying Leibnitz's rule for differentiation, we obtain

$$p(m,T)=\sum_{n=0}^{m}p_{m-n}^{(s)}p_n^{(h)}, \tag{40}$$

where

$$p_{m-n}^{(s)}=\frac{(-1)^{m-n}}{(m-n)!}\left[\frac{d^{m-n}}{ds^{m-n}}(Q_1Q_2)\right]_{s=1}, \tag{41}$$

$$p_n^{(h)}=\frac{(-1)^n}{n!}\left[\frac{d^n}{ds^n}\exp(-[f_1(s,T)+f_2(s,T)])\right]_{s=1} \tag{42}$$

are the functions associated with the SAOB and coherent component of the homodyne field, respectively. Evaluation of $p_{m-n}^{(s)}$ and $p_n^{(h)}$ can be carried out by following a procedure similar to that outlined in Refs. [8,9] for the homodyne degenerate parametric oscillator field. For the phase $\phi=0$ we find that $p(m,T)$ is super-Poissonian and for a very large value of $\overline{n}_l$ it approaches a Poissonian distribution. For the phase $\phi=180^0$, depending on the value of $\overline{n}_l$, it can show both sub- or super-Poissonian behavior. We discuss the behavior of $p(m,T)$ further in terms of its moments.

Factorial moments of the photoelectron count distribution can also provide information about the quantum statistical properties of the electromagnetic field. The lth (l a positive integer) order factorial moment of the photoelectron-counting distribution is defined by

$$\langle m^{(l)}\rangle=\sum_{m=1}^{\infty}m(m-1)\ldots(m-l+1)p(m,T), \tag{43}$$

where, for simplicity, we have suppressed the dependence of the moments on the counting interval T. Once $p(m,T)$ is known, factorial moments can be obtained from Eq. (43). They can also be obtained directly from the generating function as

$$\langle m^{(l)}\rangle=(-1)^l\left[\frac{d^l}{ds^l}G(s,T)\right]_{s=0}. \tag{44}$$

Substituting the expression for $G(s,T)$ from Eq. (29) into Eq. (44), and once again applying Leibnitz's rule for differentiation, we obtain

$$\langle m^{(l)}\rangle=\sum_{j=0}^{l}\frac{l!}{j!(l-j)!}\langle m^{(l-j)}\rangle_s\langle m^{(j)}\rangle_h, \tag{45}$$

where

$$\langle m^{(l-j)}\rangle_s=(-1)^{l-j}\left[\frac{d^{l-j}}{ds^{l-j}}(Q_1Q_2)\right]_{s=0}, \tag{46}$$

$$\langle m^{(j)}\rangle_h=(-1)^j\left[\frac{d^j}{ds^j}(\exp-[f_1(s,T)+f_2(s,T)])\right]_{s=0}. \tag{47}$$

These factorial moments can be used to characterize the nature of the field. For a classical field, the factorial moments of photon counting distribution must satisfy the following inequality [10]:

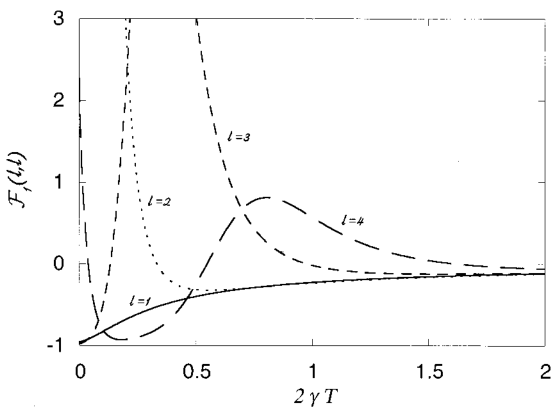

FIG. 2. The parameter $F(l,l)$ as a function of $2\gamma T$ for $l=1$ to 4. Parameters are $\overline{n}=0.010\,46$, $\overline{n_l}=0.01$, $n_0=10^3$, $C=5$, $\phi=\pi$, and $\mathcal{T}=0.5$. $F(l,l)<0$ shows nonclassical effects.

$$\mathcal{F}_k(l,j)=\left[\frac{\langle m^{(l+k)}\rangle\langle m^{(l-k)}\rangle}{\langle m^{(l)}\rangle\langle m^{(j)}\rangle}-1\right]\geqslant 0, \tag{48}$$

where i, j, and k are positive integers satisfying $l\geqslant j\geqslant k$. For quantum fields this can become negative. Therefore, $\mathcal{F}_k(l,j)<0$ provides a signature for the nonclassical nature of the field [10]. Note that the well-known Mandel parameter $Q=[\langle m^2\rangle-\langle m\rangle^2]/\langle m\rangle=\langle m\rangle\mathcal{F}_1(1,1)$. Since $\langle m\rangle$ is positive, $\mathcal{F}_1(1,1)<0$ indicates the sub-Poissonian behavior of the photon-counting distribution.

In Fig. 2 we have plotted $\mathcal{F}_1(l,l)$ as a function of the counting time interval for atomic cooperative parameter $C=5$, for several values of l. The curves shown in the graph are for the case in which the SAOB field and the local oscillator field are π out of phase and superimposed at a 50–50 beam splitter. This choice of phase allows partial removal of rather large coherent background in the SAOB by destructive interference with the LO field at the beam splitter, and therefore enhances the nonclassical effects. The parameter $\mathcal{F}_1(1,1)(=Q/\langle m\rangle)$ stays negative for all counting times reflecting sub-Poissonian statistics of the homodyne field. For $l=2$ and 4, $\mathcal{F}_1(l,l)$ is positive for short counting intervals but becomes negative for large counting intervals. The parameter $\mathcal{F}_1(3,3)$ is nearly -1 for short counting times indicating a maximum possible nonclassical effect. With an increase in counting time it becomes positive and reaches a positive maximum before decreasing and becoming negative for long counting time intervals.

Higher order sub-Poissonian and super-Poissonian behavior of light can also be characterized by the parameter S_l, which can be expressed in terms of normalized factorial moments as [13]

$$S_l=\frac{\langle m^{(l)}\rangle}{\langle m\rangle^l}-1. \tag{49}$$

For higher-order super-Poissonian statistics $S_l>0$, whereas for sub-Poissonian statistics, $S_l<0$. Since for a classical field

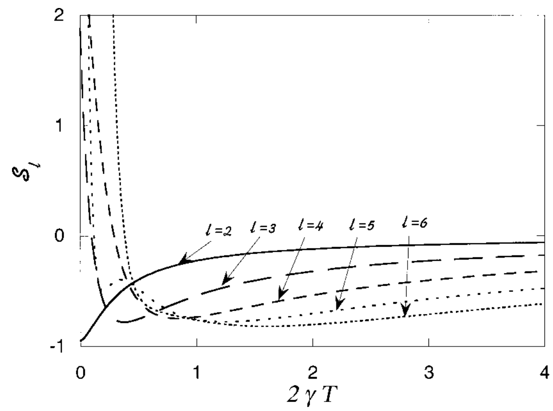

FIG. 3. The parameter S_l as a function of $2\gamma T$ for $l=2$ to 6. Parameters are $\overline{n}=0.010\,46$, $\overline{n_l}=0.01$, $n_0=10^3$, $C=5$, $\phi=\pi$, and $\mathcal{T}=0.5$. $S_l<0$ shows second- and higher-order sub-Poissonian statistics.

$S_l\geqslant 0$, *negative* values of S_l are the signature of a nonclassical field. Higher-order moments are directly measurable in photon-counting experiments.

In Fig. 3 we have plotted S_l for values of l ranging from 2 to 6 as a function of counting time for the relative phase $\phi=180°$. The parameters chosen for this figure are the same as those used for Fig. 2. We see that for these parameters $S_2(=Q/\langle m\rangle)$ is negative for all times reflecting the sub-Poissonian behavior of the light beam. The parameters S_3–S_6, on the other hand, are positive for short counting times reflecting higher-order super-Poissonian behavior. As the counting interval T increases, all S_l for $l=3$–6 become negative indicating that the homodyne field changes from super-Poissonian to sub-Poissonian even to higher orders. Each of these curves reaches a negative minimum and then starts increasing but remains negative for large counting times. The minimum shifts to longer counting times as the order l increases. It is worth noting that for large counting intervals, the higher-order sub-Poissonian character is even more pronounced than the second-order sub-Poissonian behavior based on the Q parameter. For very large counting times, S_l approaches zero indicating Poissonian statistics of the HSAOB field in this limit as expected for long counting times.

B. Waiting-time distribution

Another function to characterize photoelectron statistics is the waiting-time distribution $w(T)$, which is the probability of recording a time interval T between two successive photodetections. Since $w(T)$ involves separation between two successive photons, it is suitable for developing a physical picture of photon sequences in time and defining bunching and antibunching. Antibunching refers to the tendency of photons to be separated from one another in time and bunching refers to the tendency of photons to be bunched together in time. For an antibunching sequence the probability of detecting two photons in coincidence is smaller than that for coherent light [14]. This means that for antibunching, $w(0)<w_c(0)$, where $w_c(T)$ $(=\eta\langle I\rangle\exp[-\eta\langle I\rangle T])$ is the waiting-

time distribution for coherent light and $\langle I\rangle$ is the average intensity. For coherent light, $w_c(0)/\eta\langle I\rangle=1$ and the most probable waiting time is zero. In an antibunched photon, sequence photons are less bunched in time than photons in coherent light. Thus for an antibunched photon sequence

$$w(0)/\eta\langle I\rangle<1. \tag{50}$$

Antibunching is also discussed in terms of the second-order intensity correlation function $g^{(2)}(T)$ [15]. The difference between the waiting-time distribution $w(T)$ and $g^{(2)}(T)$ is that $w(T)$ refers to the detection of the two successive photons, whereas $g^{(2)}(T)$ refers to the detection of any two photons, irrespective of what happens in the interval $[0,T]$.

The waiting-time distribution for the HSAOB field is evaluated by differentiating the generating function given in Eq. (29) with respect to time as [8,9]

$$w(T)=\left[\frac{1}{\eta\langle I\rangle}\frac{d^2}{dT^2}G(s,T)\right]_{s=1}. \tag{51}$$

The average intensity $\langle I\rangle$ for the HSAOB field is obtained from Eq. (24) and the correlations in Eqs. (17) and (18), and is

$$\langle\hat{I}\rangle=2\gamma n_0\Bigg[\bar{n}\mathcal{T}+\bar{n}_l\mathcal{R}+2\sqrt{\bar{n}\bar{n}_l}\sqrt{\mathcal{T}\mathcal{R}}\cos\phi + \frac{\mathcal{T}\gamma C\bar{n}}{2n_0(1+\bar{n})}\left(\frac{1}{\lambda_2}-\frac{(1-2\bar{n})}{(1+\bar{n})^2\lambda_1}\right)\Bigg]. \tag{52}$$

Note that the average intensity depends on phase ϕ. It is maximum when $\phi=0$ due to constructive interference, and minimum when $\phi=\pi$ due to destructive interference. We know that for $\mathcal{T}=1$ only the light from the SAOB passes through the beam splitter and hence the waiting-time distribution of the superposed field is that of the SAOB, whereas for $\mathcal{T}=0$ we have only the light from the LO and the waiting-time distribution of the superposed field is that for a coherent light. For a value of $\mathcal{T}$ between these two extrema, it is possible to see bunching and antibunching by varying $\bar{n}$, $\bar{n}_l$, and ϕ.

In Fig. 4 we show the waiting-time distribution as a function of time for phase $\phi=\pi$, unit efficiency of detection, and several values of $\bar{n}_l$. The waiting-time distribution for the coherent field marked (e) decreases exponentially. For curves (a)–(d) all the parameters except $\bar{n}_l$ are kept fixed. A very small change in $\bar{n}_l$ causes a significant change in the waiting-time distribution. For curve (a) the waiting-time distribution shows a two-peak structure. For this curve, $w(0)/\eta\langle I\rangle$ is greater than unity reflecting bunching. With increase in time the waiting-time distribution almost vanishes at a nonzero delay time. It then increases and reaches a maximum value before decreasing to zero for large delays. As $\bar{n}_l$ increases [curve (b)] the ratio $w(0)/\eta\langle I\rangle$ decreases and shows antibunching. For this particular value of $\bar{n}_l$, we still see a two-peak structure. For larger values of $\bar{n}_l$ [curve (c)] the ratio

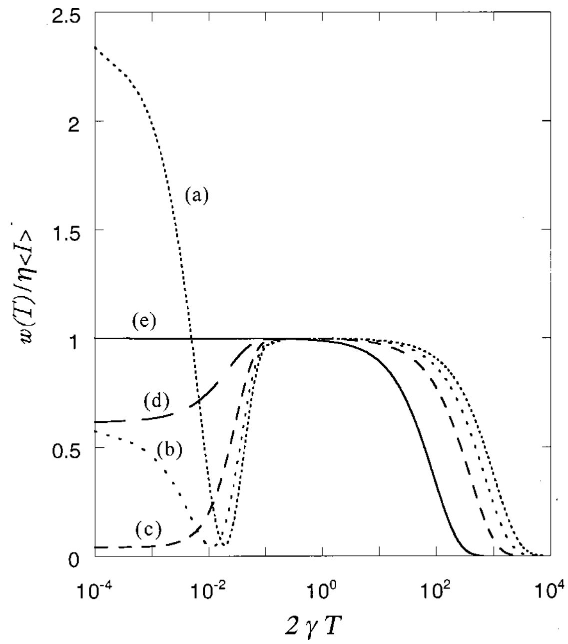

FIG. 4. The normalized waiting-time distribution $w(T)$ as a function of $2\gamma T$ for $\eta=1$, $n_0=10^3$, $C=50$, the LO mean photon number $\bar{n}=0.01$, beam splitter angle $\mathcal{T}=0.5$, and phase angle $\phi=\pi$. These plots show the effect of increasing the LO mean photon number $\bar{n}_l=$ (a) 0.010 28, (b) 0.010 34, (c) 0.010 46, and (d) 0.010 97. Curve (e) is the waiting-time distribution for coherent light with the same mean intensity as that for curve (d).

$w(0)/\eta\langle I\rangle$ is almost zero, reflecting maximum antibunching. For this curve, $w(T)$ has a single peak structure leading to a regular photon sequence. With further increase in $\bar{n}_l$ [curve (d)] the ratio $w(0)/\eta\langle I\rangle$ is nonzero but still less than one indicating antibunching. With an increase in the delay time, the waiting-time distribution increases and shows a single peak structure. With further increase in $\bar{n}_l$, the waiting-time distribution for the HSAOB approaches that for coherent light.

All the interesting features seen in Fig. 4 can be observed if $\bar{n}_l$ is decreased below $\bar{n}=0.01$. They are also observed if $\bar{n}$ or $\mathcal{T}$ is varied keeping all other parameters fixed. It is possible to achieve a large amount of antibunching for small values of $\bar{n}$ by choosing $\bar{n}_l$ and $\mathcal{T}$ so that a coherent component of the SAOB is partially removed by destructive interference. A maximum amount of antibunching can be observed for $\phi=\pi$ as destructive interference is largest for this choice of phase. For $\bar{n}>1/2$, we find that the photon sequence for the homodyne field is always bunched.

IV. SUMMARY

In conclusion we have studied the photon statistics of the field generated by superposing the field from a two-level atomic system that shows optical bistability and a coherent field from a local oscillator at a lossless beam splitter. Our analysis is based on the quantum dynamical equations of motion for the field when a two-level atom is placed inside a coherently driven cavity in the good cavity limit [2]. The field from a cavity containing N two-level atoms can also be described by similar dynamical equations if the atomic cooperativity parameter C is appropriately defined. Therefore, our analysis of the photon statistics of the homodyne field presented in this paper is valid for both single-atom and multiatom systems.

By applying classical inequalities expressed in terms of the factorial moments [10,14], we have identified new regimes for the homodyne field, where the nonclassical nature is reflected in moments higher than the second. Nonclassical features of the field are strongest when the relative phase difference between SAOB and LO fields is 180° and the mean photon numbers for the LO and the SAOB are comparable but not exactly equal.

Quantum interference between the SAOB and LO fields also introduces new features in the waiting-time distribution, which for classical fields must obey the inequality $w(0)/\eta\langle I\rangle > 1$. The homodyne field violates this inequality. In particular, the homodyne field has a diminished and sometimes near-zero probability of detecting two successive photons separated by nonzero delay time.

Antibunching and sub-Poissonian behavior for the HSAOB is due to an interference between the quantum noise and the coherent field. The field from the SAOB has a very large coherent component, which suppresses nonclassical effects such as antibunching or sub-Poissonian statistics. Homodyning the SAOB field with the local oscillator with $\phi = 180°$ allows us to remove the coherent background of the SAOB by destructive interference at the beam splitter. It is worth mentioning that if the coherent component is completely removed, the SAOB field exhibits bunching and shows higher-order super-Poissonian statistics. A small amount of coherent component is essential for the enhancement of the nonclassical effects. This occurs when the coherent component is comparable and out of phase with the noise term of the SAOB. Nonclassical effects discussed here tie interference between quantum noise and a coherent field, a wave feature, to the photon-counting process that is understood from the particle viewpoint. The results of this paper, therefore, can be considered as a manifestation of the intertwining wave-particle duality of the field.

ACKNOWLEDGMENTS

This work was supported in part by the Office of Naval Research and Arkansas Science and Technology Authority. D.E. acknowledges partial support from ICSC World Laboratory.

[1] C.M. Savage and H.J. Carmichael, IEEE J. Quantum Electron. **QE-24**, 1495 (1988).
[2] C. Wang and R. Vyas, Phys. Rev. A **54**, 4453 (1996).
[3] P.D. Drummond and D.F. Walls, Phys. Rev. A **23**, 2563 (1981); H.J. Carmichael, D.F. Walls, P.D. Drummond,and S.S. Hassan, *ibid.* **27**, 3112 (1983); L. A. Lugiato, in *Progress in Optics*, edited by E. Wolf (North-Holland, Amsterdam, 1984), Vol. XXI, pp. 69–216.
[4] H.J. Carmichael, Phys. Rev. A **33**, 3262 (1985); H.J. Carmichael, J.S. Satchell, and S. Sarkar, *ibid.* **34**, 3166 (1986); S. Sarkar and J.S. Satchell, Europhys. Lett. **3**, 797 (1987).
[5] A. Bandilla and H.H. Ritze, Opt. Commun. **28**, 126 (1979); H.H. Ritze and A. Bandilla, *ibid.* **28**, 241 (1979).
[6] G. S. Holliday and S. Singh, in *Coherence and Quantum Optics VI*, edited by J. H. Eberly, L. Mandel, and E. Wolf (Plenum, New York, 1990), p. 509; Y. Qu, M. Xiao, G.S. Holliday, S. Singh, and H.J. Kimble, Phys. Rev. A **45**, 4932 (1992).
[7] R. Vyas, C. Wang, and S. Singh, Phys. Rev. A **54**, 2391 (1996).
[8] A.B. Dodson and Reeta Vyas, Phys. Rev. A **47**, 3396 (1993).
[9] R. Vyas and S. Singh, Phys. Rev. A **38**, 2423 (1988); Opt. Lett. **14**, 1110 (1989); Phys. Rev. A **40**, 5147 (1989); R. Vyas, and A.L. DeBrito, *ibid.* **42**, 592 (1990).
[10] R. Vyas and S. Singh, Phys. Rev. A **62**, 033803 (2000).
[11] C. Wang and R. Vyas, Phys. Rev. A **51**, 2516 (1995); **55**, 823 (1997).
[12] P.D. Drummond and C.W. Gardiner, J. Phys. A **13**, 2353 (1980).
[13] D. Erenso, R. Vyas, and S. Singh (unpublished).
[14] R. Vyas and S. Singh, J. Opt. Soc. Am. B **17**, 634 (2000).
[15] R. Loudon, Rep. Prog. Phys. **43**, 913 (1980); H. Paul, Rev. Mod. Phys. **54**, 1061 (1982).